

## Photometry of Saturated Stars with Machine Learning

DOMINIK WINECKI<sup>1</sup> AND CHRISTOPHER S. KOCHANEK<sup>2,3,\*</sup>

<sup>1</sup>*Department of Computer Science and Engineering, The Ohio State University, Columbus, OH 43210, USA*

<sup>2</sup>*Department of Astronomy, The Ohio State University, 140 W. 18th Ave., Columbus, OH 43210, USA*

<sup>3</sup>*Center for Cosmology and AstroParticle Physics, The Ohio State University, 191 West Woodruff Ave., Columbus, OH 43210, USA*

### ABSTRACT

We develop a deep neural network (DNN) to obtain photometry of saturated stars in the All-Sky Automated Survey for Supernovae (ASAS-SN). The DNN can obtain unbiased photometry for stars from  $g \simeq 4$  to 14 mag with a dispersion (15%-85%  $1\sigma$  range around median) of 0.12 mag for saturated ( $g < 11.5$  mag) stars. More importantly, the light curve of a non-variable saturated star has a median dispersion of only 0.037 mag. The DNN light curves are, in many cases, spectacularly better than provided by the standard ASAS-SN pipelines. While the network was trained on  $g$  band data from only one of ASAS-SN's 20 cameras, initial experiments suggest that it can be used for any camera and the older ASAS-SN V band data as well. The dominant problems seem to be associated with correctable issues in the ASAS-SN data reduction pipeline for saturated stars more than the DNN itself. The method is publicly available as a light curve option on ASAS-SN Sky Patrol v1.0.

### 1. INTRODUCTION

Projects such as the All-Sky Automated Survey for Supernovae (ASAS-SN, Shappee et al. 2014, Kochanek et al. 2017, Hart et al. 2023), the Asteroid Terrestrial-impact Last Alert System (ATLAS, Tonry et al. 2018a) and the Zwicky Transient Facility (ZTF, Bellm et al. 2019) currently monitor all (ASAS-SN and ATLAS) or large fractions (ZTF) of the visible sky and provide public access to their data. For ASAS-SN, this consists of its catalog of variable stars (Jayasinghe et al. 2019), ASAS-SN Sky Patrol (Kochanek et al. 2017), which will provide an uncensored light curve for any user requested sky coordinate, and ASAS-SN Sky Patrol v2.0 (SP2, Hart et al. 2023), which provides continuously updated light curves of roughly 100 million sources from asteroids to stars and quasars. In the near future, the Vera Rubin Observatory (e.g., Ivezić et al. 2019) will provide ZTF-like coverage and cadence for far fainter sources.

Professional astronomy has lost, however, the ability to monitor the bright sky – the need for both funding and efficient operations drive projects towards fainter and more numerous sources. Yet these very bright sources are the ones which will have the best stellar spectroscopic observations from projects like SDSS/APOGEE (e.g., Abdurro'uf et al. 2022) or Gaia

(e.g., Gaia Collaboration et al. 2023) including either indications of binarity or full orbital solutions.

The problem is that charge coupled device (CCD) detectors have a finite dynamic range above which a pixel is saturated. A typical dark time All-Sky Automated Survey for Supernovae (ASAS-SN) image has a sky background of  $\sim 200$  counts and saturates at  $\sim 60,000$  counts. The PSF has a FWHM of roughly 2 pixels (Shappee et al. 2014, Kochanek et al. 2017), leading to a point source dynamic range of roughly 7 magnitudes from  $g \sim 11.5$  to  $g \sim 18.5$  mag. This leaves some  $\sim 10^6$  stars that are saturated in ASAS-SN observations. The excess charge of the saturated pixels then bleeds into pixels along the read direction of the detector.

ASAS-SN inherited from the original All-Sky Automated Survey (ASAS, Pojmanski 2002) one method of trying to obtain photometry of saturated stars. The pipeline tries to identify the flux in the bleed trails of the saturated stars and then adds a Gaussian with that flux at the star's location. The bleed trails are then replaced by linear interpolation of the adjacent, unsaturated pixels. This approach has also been applied to Swift/UVOT data by Page et al. (2013). As shown by some of the examples in Kochanek et al. (2017), this procedure frequently works surprisingly well. An alternative approach is to model the unsaturated wings of the PSF (e.g., Su et al. 2022, Zhou et al. 2023).

Here, we experiment with a new approach, namely, training a deep neural network (DNN) to do pho-

\* Email: kochanek.1@osu.edu

tometry of saturated stars. Convolutional neural networks (CNNs) have been used successfully for a range of astronomical problems, such as star–galaxy classification (Kim & Brunner 2017), transient classification (Qu et al. 2022) and photometric redshifts (Pasquet et al. 2019). There have been some applications of CNNs to photometry (Yang et al. 2023; Yuan et al. 2023) but not to the specific problem of saturated star photometry. Here we use DNNs because they retain the position information, which seems relevant to photometry of an already identified object. The theory is that a network can simply learn the sensor-specific behavior for stars of different levels of saturation and then predict the true brightness. In Section 2 we describe the construction of the training set, and in Section 3 we describe the model and the training process. We present the results in Section 4 with comparisons to the results produced with aperture photometry on subtracted images by ASAS-SN Sky Patrol v2.0 (Hart et al. 2023). We discuss the results, known problems, potential solutions and possible future improvements in Section 5.

## 2. TRAINING DATA

We selected stars from Gaia DR3 (Gaia Collaboration et al. 2016, Gaia Collaboration et al. 2023) that were observed by the “bi” camera of the ASAS-SN Bohdan Paczynski mount at CTIO in Chile. We selected a random 40,000 non-variable stars (based on Gaia DR3, Eyer et al. 2023) over the sky per one magnitude wide bin starting at  $G = 2$  mag. This provides a training set roughly uniformly distributed in magnitude. Obviously, the very brightest bins have fewer than 40,000 stars and so we were simply including all available stars. We kept stars observed by bi, with defined  $G$ ,  $B_P$  and  $R_P$  magnitudes.

Each target then has 100s of epochs of ASAS-SN observations, so we randomly selected  $\sim 4$  images per target and extracted a 21 pixel square “postage stamp” image of the target. We used single exposures interpolated to the astrometric frame of the reference image. Only images flagged as having been taken in good conditions were used and the postage stamp edges had to be at least 50 pixels from the detector edges. We generated  $\sim 332$  thousand postage stamps spanning  $G = 3$  to 15 mag.

We predict the  $g$  band magnitudes from the Gaia DR3 magnitudes because the Gaia magnitudes homogeneously span the full range we consider. We first applied the Gaia EDR3 saturation corrections from Riello et al. 2021 (these affect  $G < 8$  for  $G$ ,  $G < 3.94$  for  $B_P$  and  $R_P < 3.45$  for  $R_P$ ) and estimate the  $g$ -band magnitude from the corrected  $G$ ,  $B_P$  and  $R_P$  magnitudes follow-

ing Riello et al. (2021). We then convert to the estimated counts in an image using the zero point  $Z$  of the ASAS-SN reference image and the mean transparency correction  $t$  between fluxes on the reference image and the target image determined by ISIS (Alard & Lupton 1998, Alard 2000) as part of the standard ASAS-SN image subtractions (the values in `sum_kernel`). This gives predicted counts of

$$\log N_s = -0.4(g - Z) - \log t. \quad (1)$$

The ASAS-SN point spread function has a FWHM of roughly 16 arcsec. At this resolution, the flux in any ASAS-SN photometric aperture can be a blend of the fluxes from multiple stars. This is not important for the brightest stars, but becomes increasingly important for fainter stars, particularly at lower Galactic latitudes. To mitigate this, we found all  $G < 20$  mag Gaia DR3 stars within 1 arcmin of each target star. We computed a  $G$ -band flux correction  $f_c$  factor to go from the flux of the target star to the total flux of all stars within 8 arcsec. Assuming that the network will “learn” about background subtraction we need to correct this contaminating flux for the median stellar background flux contribution,  $b_c$ , to the signal region. Hence, we rescale the prediction for the number of counts as

$$N_s \rightarrow N_s(1 + f_c) - b_c. \quad (2)$$

When we added bias subtraction to the ASAS-SN pipelines, we started to damage the cores of the images of saturated stars, a problem that remains to be fixed. Such damaged stars are identifiable by the presence of pixels that are exactly unity because the final consequence of the damage is that the modified ASAS pipeline declares them to be bad pixels and resets them to unity. Postage stamps with more than four such pixels are rejected for training and validation.

## 3. METHODS

In our dataset, the target star never covered more than a few pixels in any direction, even at the highest brightness levels. As a pre-processing step, we reduced the analyzed region of each postage stamp to a 5 pixel radius circle around the center. This is to help focus the model training on the relevant region and to give less context for a model to memorize. A sampling of the brightest stars found that a 5 pixel radius would capture most visible detail with a  $\sim 1$ -2 pixel margin, as shown in Fig. 1.

As an easy way to expand the training set, we also considered reflections of the postage stamps, adding three new postage stamps flipped horizontally, vertically, or

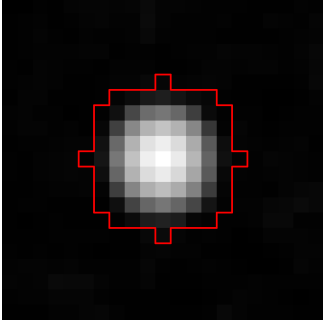


**Figure 1.** A log scale image of the postage stamp of a 99.9th percentile bright star with a red contour drawn to show which pixels are used in our model.

both. This grows the training set from  $\sim 332$  thousand stamps to  $\sim 1.33$  million stamps. To the extent that the ASAS-SN point spread function is not circularly symmetric, this is like moving the postage stamp to the corresponding reflection of its position on the detector. We expected this to be a safe way of trivially multiplying the training set. We tracked the results for both the original and permuted orientations and were unable to find significant differences in the results.

Neural networks operate on the data turned into “tensor data” which is simply a one dimensional array. We can also append metadata to the end of the training data, where we experimented with adding the reference image zeropoint  $Z$  and the estimated sky brightness of the individual image  $S$ . We discuss other possible metadata that could be used in the discussion.

The overall training set is then divided into training (60%), testing (20%) and validation sets (20%). We were concerned about the potential for the network to memorize the expected properties of a particular star based on the pattern of surrounding background stars. To make sure this was not an issue in terms of validating the results, all images of a particular star were placed in one of the three subsamples.

#### 4. RESULTS

We carried out our analysis using PyTorch (Paszke et al. 2019), optimizing the mean squared error (MSE) loss function between the input estimate of  $\log N_s$  and the output estimate from the network. We began by experimenting with different DNN architectures. We started with 2-4 smaller 64-wide layers, but found that increasing the width led to faster convergence. We ultimately settled on 256-wide layers as increasing past this led to minimal improvements. The final architecture is shown in Fig. 2.

After selecting the architecture, we evaluated PyTorch’s Adam, AdamW, Adadelta, Adagrad, Adamax, RMSProp, and SDG optimizers. We trained each model to 150 epochs with each optimizer multiple times. The Adam optimizer had the lowest losses, with AdamW coming second. The other optimizers were less reliable for this task, with some never converging. We used the Adam optimizer of Kingma & Ba (2017) for our final models, with a learning rate of 0.0001 and a batch size of 128. We trained 24 models using this architecture including the hyper-parameters in the training and selected the one with the best MSE.

The performance of the standard model for the verification data set is shown in Fig. 3. The results show negligible bias over 10 magnitudes (a factor of  $10^4$  in flux) from  $g \simeq 4$  mag to  $g = 14.5$  mag. The median difference is  $-0.004$  mag, with a clear bias appearing only for the  $g > 14$  mag stars. The magnitude differences encompassing 68% and 95% of the stars are 0.12 and 0.34 mag and the RMS dispersion is 0.168 mag.

We also considered several possible elaborations. First, we considered whether ensemble results would perform better than the best model. For example, if we defined the ensemble model as the average of the results from the four individual models with the lowest MSE values, the RMS residual did not improve. Second, we tried averaging the results for the input image and its three permutations, but again found no significant improvement. As noted earlier, many saturated stars have pixels reset to unity due to some unanticipated consequences of adding overscan corrections to the pipeline. We built an independent network trained only on objects with at least one pixel set to unity to see if this would do better than simply mixing the two populations. This model had an RMS residual of 0.360 mag, far worse than the general analysis. We believe the small size of the resulting training set likely drives this. From this point on, we focus on our standard model.

We looked for correlations of the residuals with distance from the detector center and Galactic latitude. We examined the distance from the center because a source of a given flux produces  $\sim 50\%$  fewer counts in the extreme corners of the detectors compared to the center due to vignetting. We examined the Galactic latitude because the stellar density increases rapidly for lower absolute latitudes, so the results depend more on correctly accounting for crowding by other sources under the ASAS-SN PSF. We found no significant correlation of the residuals with either the detector location or Galactic latitude.

Fig. 3 is not really a test of our primary goal, which is to produce improved light curves rather than im-

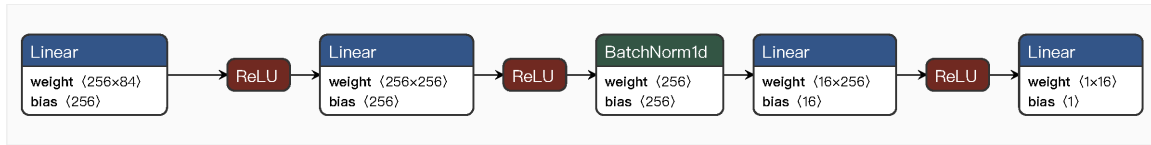
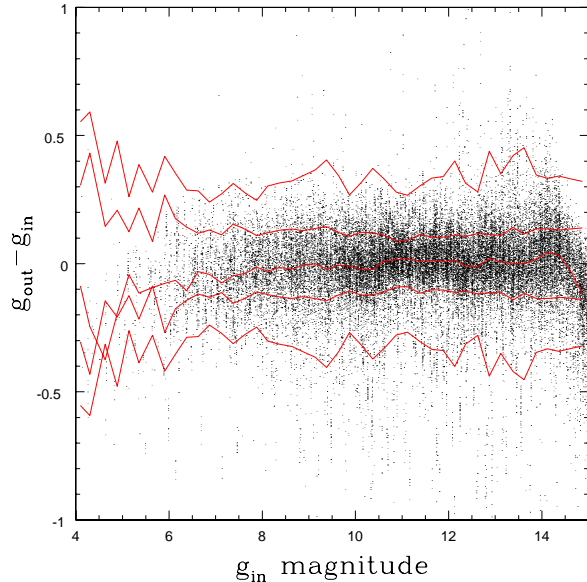


Figure 2. Final Model Architecture



**Figure 3.** The differences between the input ( $g_{in}$ ) and output ( $g_{out}$ ) magnitudes for the verification stars. The red curves show the median, 68% and 95% ranges of the differences in bins of 0.25 mag.

proved absolute photometry over the current ASAS-SN pipelines as implemented in Sky Patrol v2.0 (SP2, Hart et al. 2023). ASAS-SN epochs are generally comprised of three 90 second exposures. SP2 does aperture photometry on the co-added, subtracted images obtained for each epoch and then adds the flux of the source in the reference image. The DNN analyzes individual images since we are limited by systematic problems not photon statistics for the saturated stars. For the final DNN light curves we used the median of the results for the individual epoch images (the average if only two images, and the value if there is just one image). This procedure noticeably reduces the light curve dispersions.

To test the performance on light curves, we randomly selected 1000 (Gaia) non-varying sources uniformly in magnitude over  $8 < g < 14.5$  mag and extracted their light curves using both the best DNN model and SP2. We again limited the analysis to good images and kept only images analyzed by both pipelines. Fig. 4 compares the dispersions of the DNN and SP2 light curves with at least 50 points as a function of magnitude. The disper-

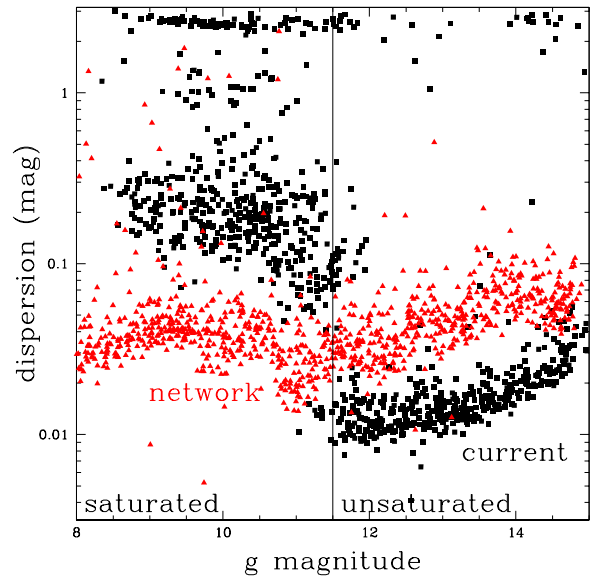


**Figure 4.** The light curve dispersions of approximately  $10^3$  non-variable sources as a function of  $g$  magnitude analyzed using the current SP2 pipeline (black squares) or by the neural network (red triangles). The dispersion is defined as one-half of the 15-85% ( $1\sigma$ ) range of the residuals about the median.

sions are defined by one-half of the 15-85% ( $1\sigma$ ) range about the light curve median. The standard pipeline has obvious problems for saturated ( $g < 11.5$ ) images, with a large jump in the scatter from a median of 0.016 mag for  $g > 11.5$  to a median of 0.22 mag for brighter sources. The band of sources with scatters above one magnitude are the ones most badly affected by the effects of the bias subtraction problem. The performance of the DNN is fairly uniform with a median scatter of 0.037 mag for the brighter sources and 0.048 for the fainter sources. A few of the high scatter outliers are high proper motion stars, but most are cases where the bleed trail correction algorithm has put the flux from the bleed trail in the wrong location. An obvious issue for future work is to explore why the DNN has three times the scatter of the standard pipeline for the unsaturated stars. Fig. 5 shows eight examples of these DNN light curves. They were selected to have 15-85% ( $1\sigma$ ) ranges about their medians of  $< 0.053$  mag, which is true for 85% of the saturated stars (see Fig. 4), but were otherwise just chosen to be the closest star to 8.0, 8.5  $\dots$  11.5 mag.

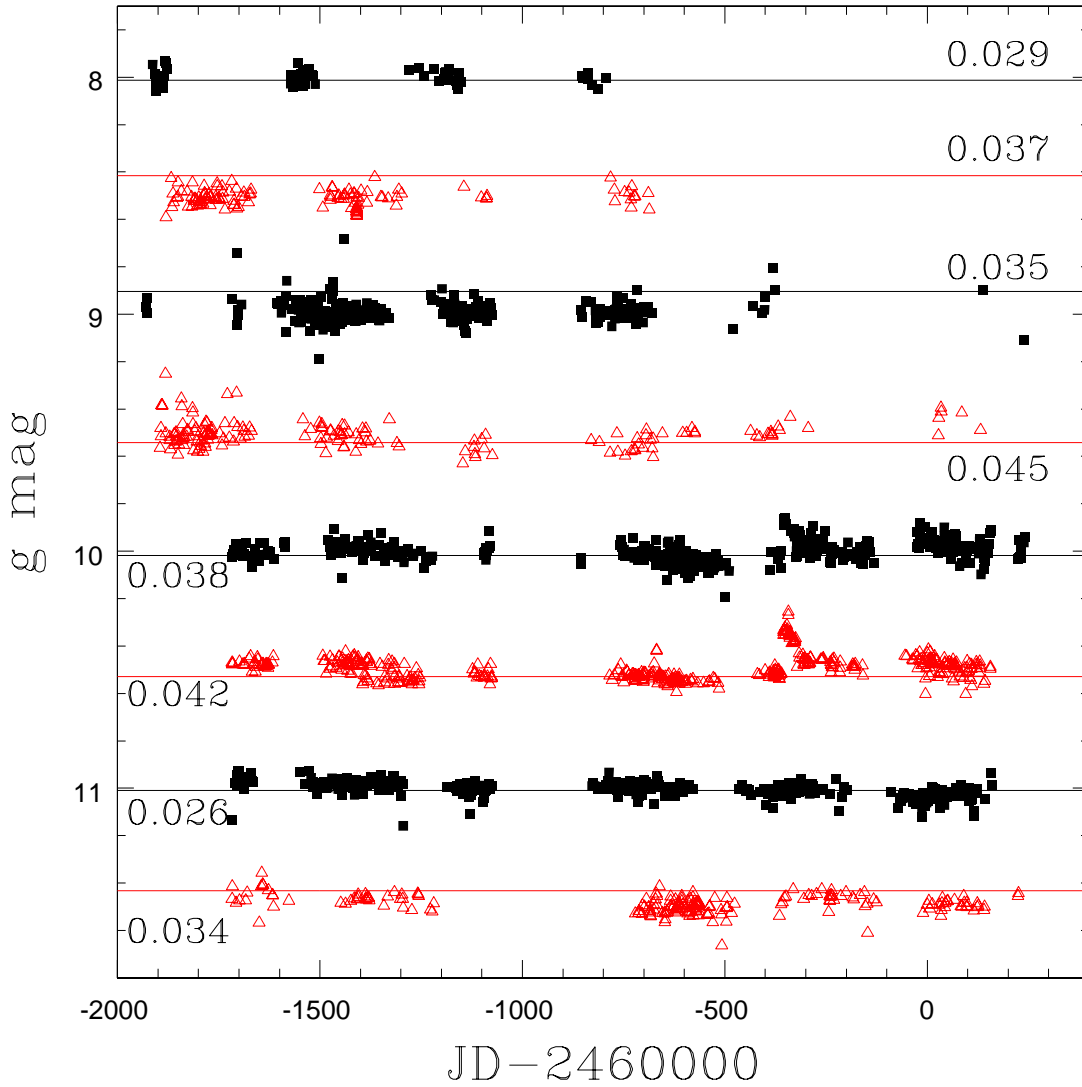


**Figure 5.** Light curves of the non-variable verification sample stars closest to  $g = 8$  mag to 11.5 mag in steps of 0.5 mag. They were also required to have 68% distribution widths less than 0.053 mag – 85% of  $g < 11.5$  mag stars have smaller dispersions. The horizontal lines are the Gaia-estimated  $g$  magnitudes. The number gives the dispersion estimated from the 15-85% ( $1\sigma$ ) range of the points about their median.

Figs. 6, 7, 8 and 9 compare the DNN light curves of Mira, Cepheid and eclipsing binaries to those from SP2. These variables were not selected to make the DNN results look good, but simply to have interesting magnitudes and amplitudes for illustrating results. The Miras illustrate the ability of the DNN analysis to smoothly track the brightness of variable stars from well below the saturation limit near  $g \simeq 11.25$  mag to significantly above it. While the SP2 light curves are frequently good, they start to produce significant outliers at the brightest magnitudes, particularly for X Oct. The examples of classical Cepheids include the extremely bright  $\ell$  Car, the still naked eye visible W Sgr and the slightly fainter

R Cru. The DNN  $\ell$  Car light curves are producing significant numbers of outliers near peak, while the SP2 light curves struggle near minimum. The W Sgr and R Cru light curves have significant numbers of faint outliers, but the DNN produces generally smoother light curves if we ignore the outliers. The DNN magnitudes are also closer to the  $g$  magnitudes predicted from the Gaia mean magnitudes. Note that since they are mean magnitudes, they should be relatively immune to any variability. The SP2 light curves are significantly fainter than the predictions and are shifted brighter by  $\sim 1$  mag in order to use the same magnitude ranges for both the DNN and SP2 light curves.

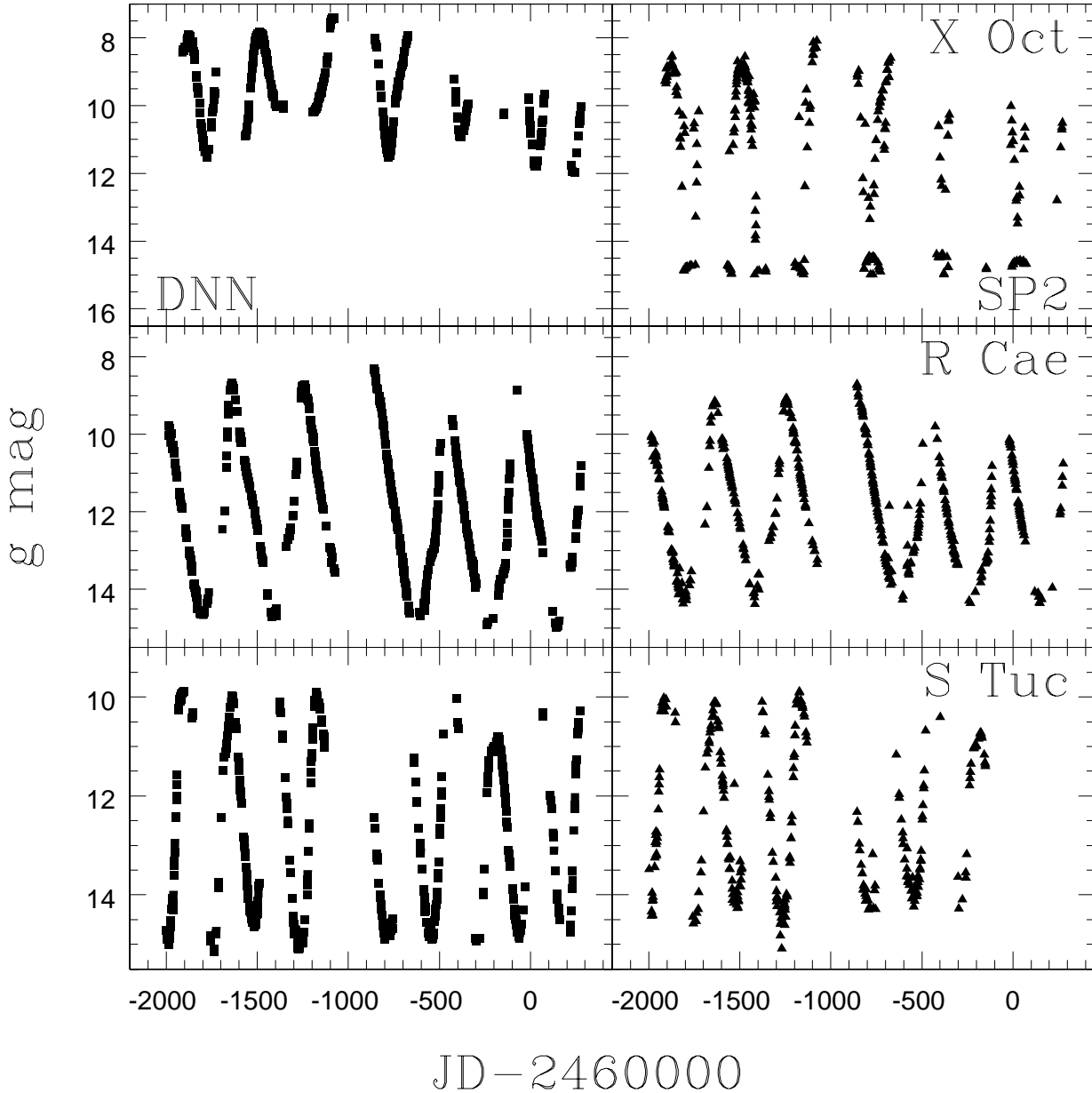


**Figure 6.** Light curves of Mira variables from the DNN analysis (left) and Sky Patrol V2.0 (right, SP2). While the saturated star corrections of the ASAS-SN pipeline produce surprisingly good results in many cases, the DNN pipeline results are smoother and have fewer outliers like the ones prominently seen for the SP2 light curve of X Oct. X Oct is also the example which is most saturated at peak brightness. The vertical scales are the same for both the DNN and SP2 light curves.

The driver of these problems for the bright Cepheids are two failure modes in the pipeline saturated star correction. One failure mode is to place the flux from the bleed trails at the wrong location, usually a relatively bright (but not nearly as bright) star lying nearby on the bleed trail. The second, which we do not understand, but appears to be the dominant failure for W Sgr, is to have not placed the missing flux anywhere. The saturated target appears to have been treated as part of

the bleed trail and filled in by interpolation across the estimated trail.

The eclipsing binary comparisons provide the most dramatic illustration of the improvements from the DNN approach - the eclipses are clearly visible in the DNN light curves and essentially invisible in the SP2 light curves. Even CY Hyi, with its fairly high amplitude and continuous variability with phase, has a barely discernable variability pattern in the SP2 light curve. The



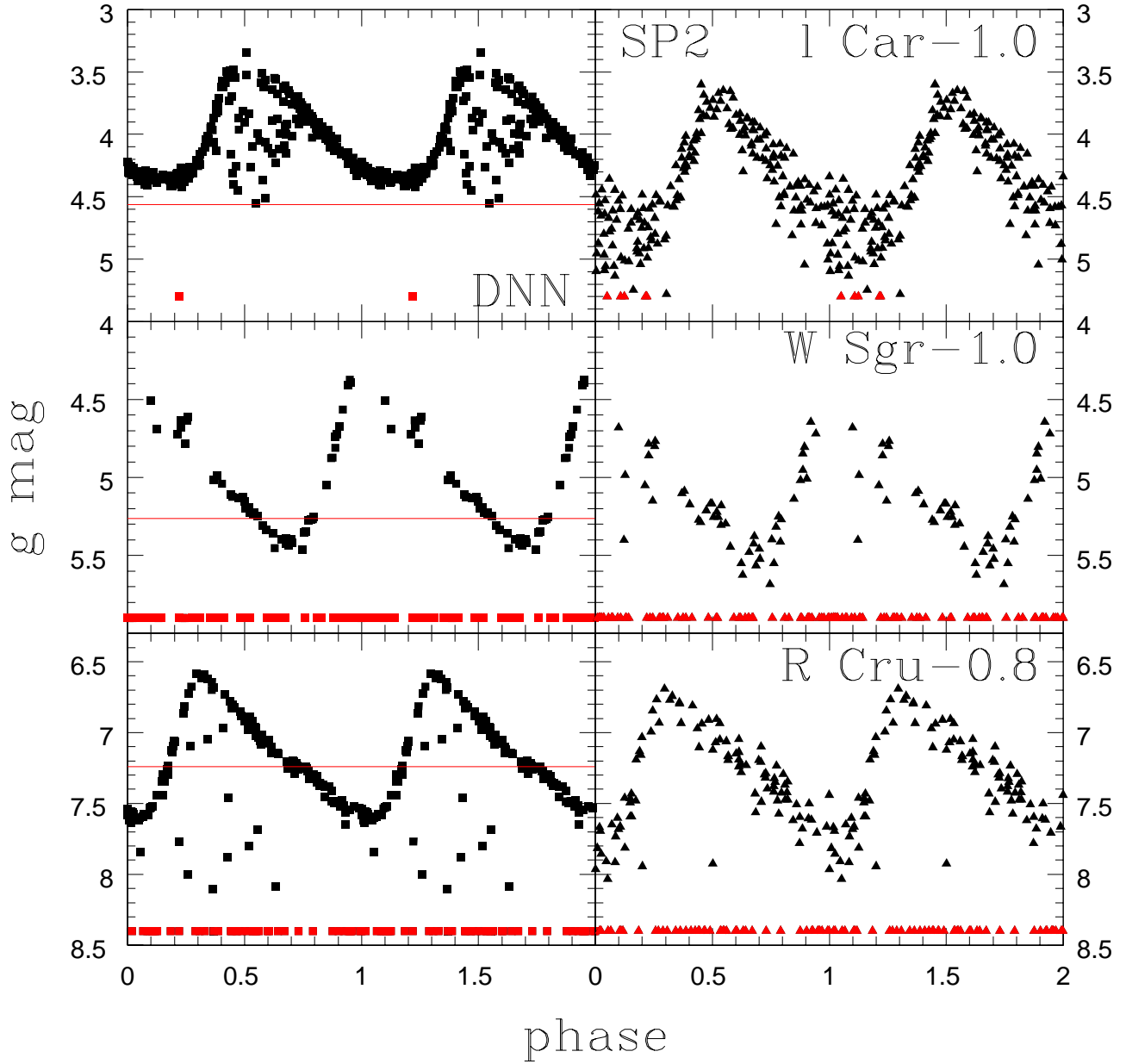


**Figure 7.** Light curves of very saturated Cepheid variables from the DNN analysis (left) and Sky Patrol V2.0 (right, SP2). The SP2 light curves are shifted to brighter magnitudes by the amount next to the variable name. The red points lying in a line along the bottom are outliers fainter than the minimum magnitudes of the panels. The horizontal red line is the  $g$  magnitude predicted from the mean Gaia magnitudes, which should be relatively close to the true mean magnitude. Both pipelines produce many faint outliers for W Sgr and R Cru, but the DNN light curves are arguably cleaner except for  $\ell$  Car at peak. The vertical scales are the same for both the DNN and SP2 light curves.

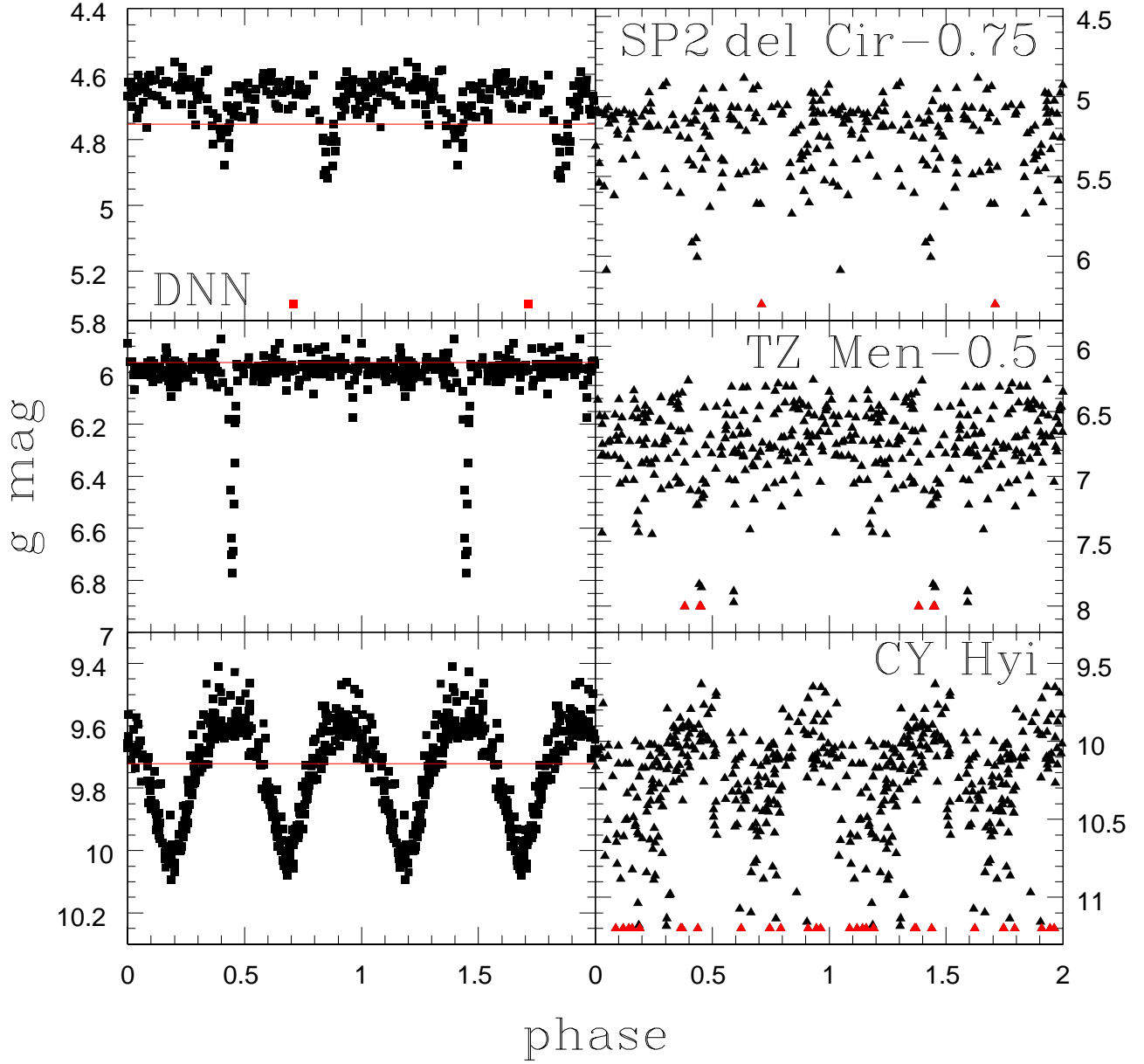


**Figure 8.** Light curves of eclipsing binaries from the DNN analysis (left) and Sky Patrol V2.0 (right, SP2). The SP2 light curves are shifted to brighter magnitudes by the amount next to the variable name. The bright magnitude limit is the same for the DNN and SP2 panels, but the magnitude range is generally much larger for the SP2 panels. The red points lying in a line along the bottom are outliers fainter than the minimum magnitudes of the panels. The horizontal red line is the  $g$  magnitude predicted from the mean Gaia magnitudes.



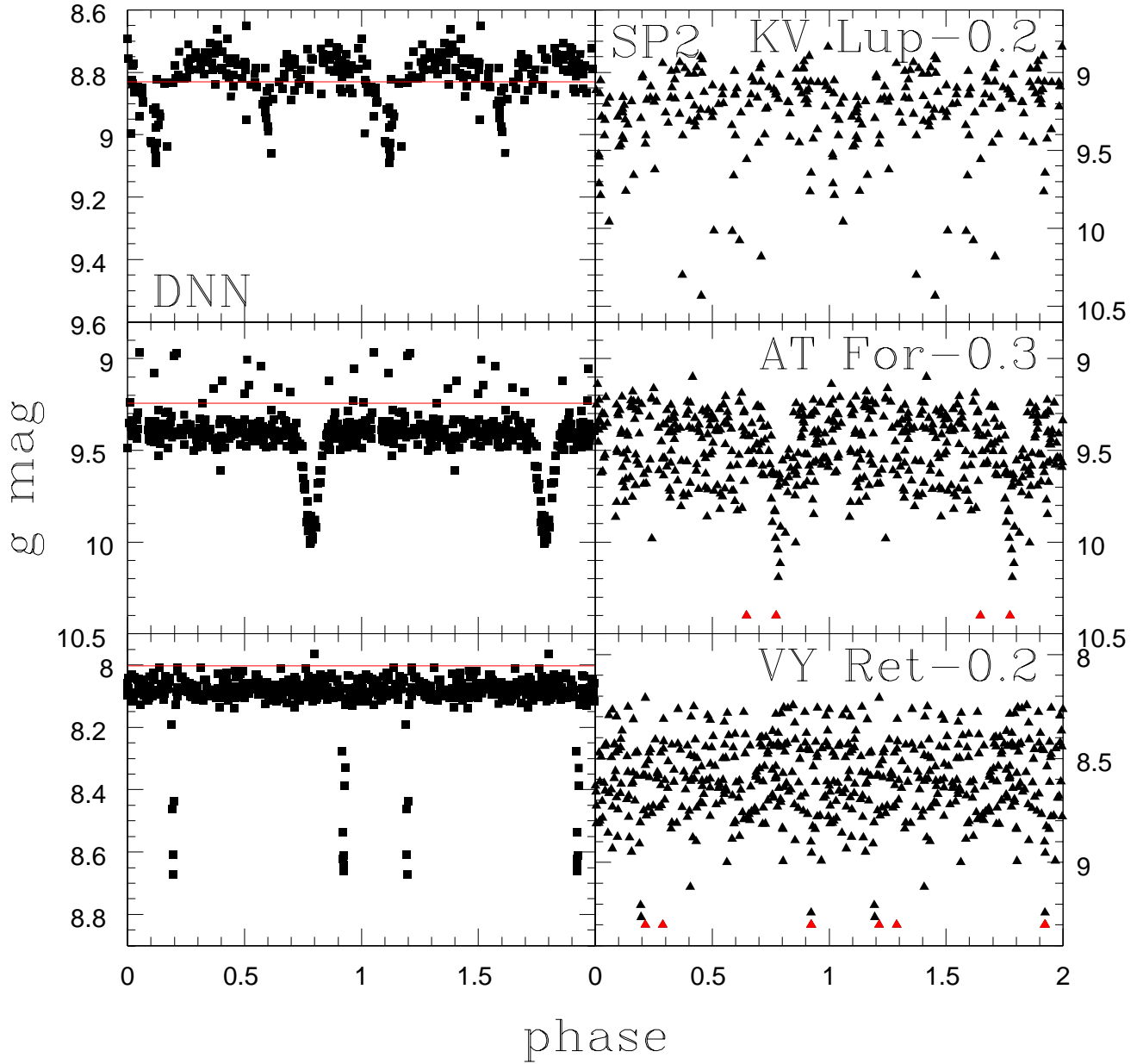


**Figure 9.** Light curves of eclipsing binaries from the DNN analysis (left) and Sky Patrol V2.0 (right, SP2). The SP2 light curves are shifted to brighter magnitudes by the amount next to the variable name. The bright magnitude limit is the same for the DNN and SP2 panels, but the magnitude range is generally much larger for the SP2 panels. The red points lying in a line along the bottom are outliers fainter than the minimum magnitudes of the panels. The horizontal red line is the  $g$  magnitude predicted from the mean Gaia magnitudes. VY Ret has a highly eccentric orbit leading to the asymmetric eclipse phases.

shallow eclipses of del Cir and KV Lup are clear for the DNN light curves, as are the very narrow eclipses of TZ Men and VY Ret. The mean DNN magnitudes are close to the predicted means, while the SP2 means are again significantly fainter than predicted. There are outliers in the DNN light curves, but most could probably be eliminated with some variant of sigma clipping.

The DNN was trained using data from only a single camera (“bi” on the Paczynski mount), while ASAS-SN is presently comprised of 20 cameras. ASAS-SN also initially used V band, while the training data was all  $g$  band photometry. As an experiment, we simply analyzed the data from all cameras and both filters for the stars in Figs. 6, 7, 8 and 9. We “inter-calibrated” the data from all the sources using a Damped Random Walk

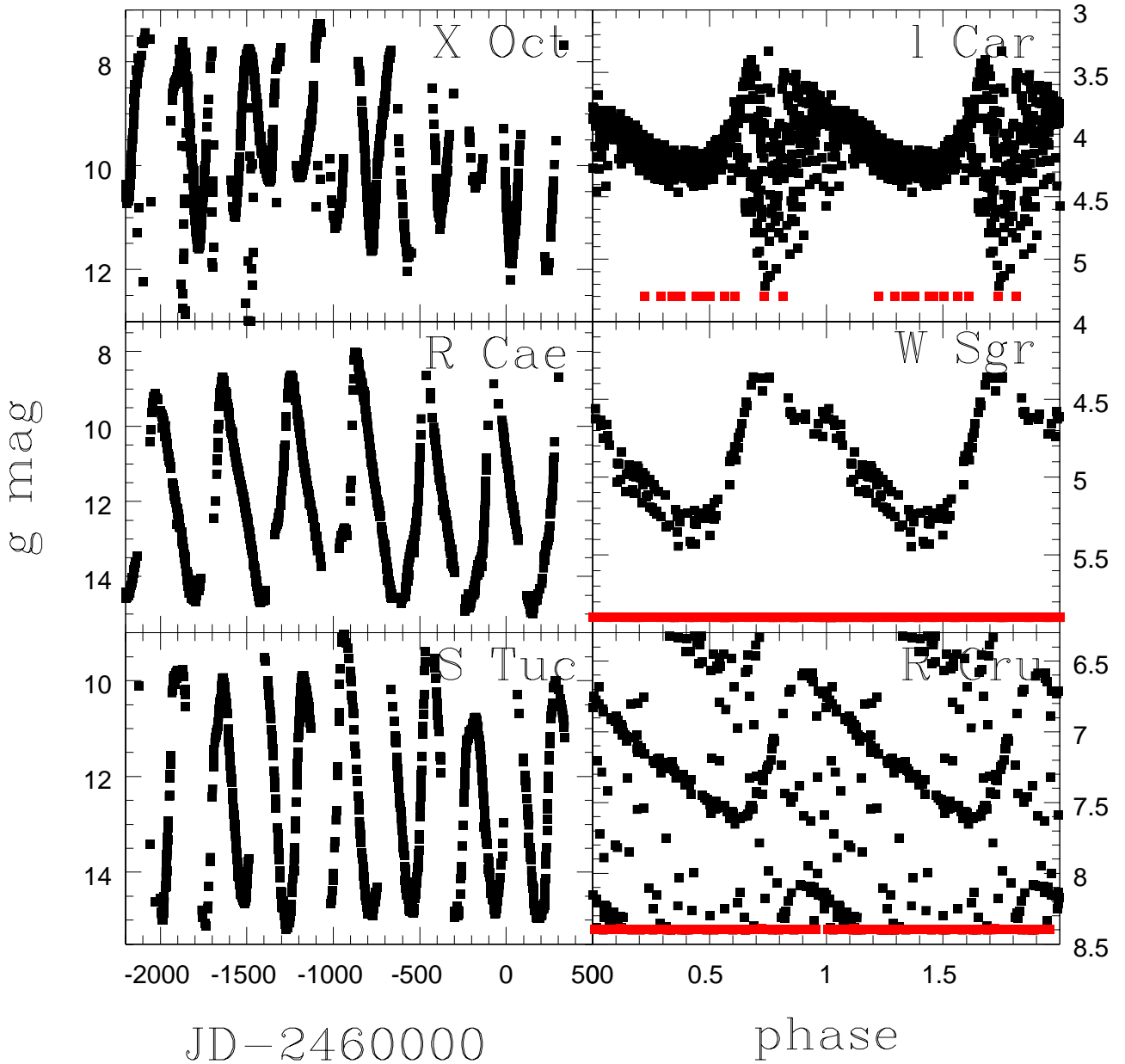


**Figure 10.** DNN light curves of the Miras and Cepheids from Figs. 6 and 7 (black squares) as compared to their DNN light curves using both V and g band data from all the ASAS-SN cameras observing each star. Outliers are marked at the bottom in red.

(DRW) Gaussian process for interpolation and solving for the best light curve means for the individual cameras and filters (these are a form of the “linear parameters” discussed in Kozłowski et al. 2010). We found we could reduce the effects of faint outliers by dropping the faintest 10% of the light curves. Each light curve was then offset by the difference between the median light curve mean and the mean for the individual camera and filter. This does assume that the variability amplitudes and light curves shapes are identical for the two filters,

but it also the most extreme test for seeing how crucial it will be to individually train by camera and filter.

Figs. 10 and 11 show the results. They are generally very good, suggesting that the current network can simply be applied generally and that we could train one DNN using data from all cameras and filters. There are outliers such as those seen for X Oct, and all the data is struggling with the bright Cepheids from Fig. 10. The biggest failure is for R Cru, where the huge number of outliers has confused the inter-calibration procedure.

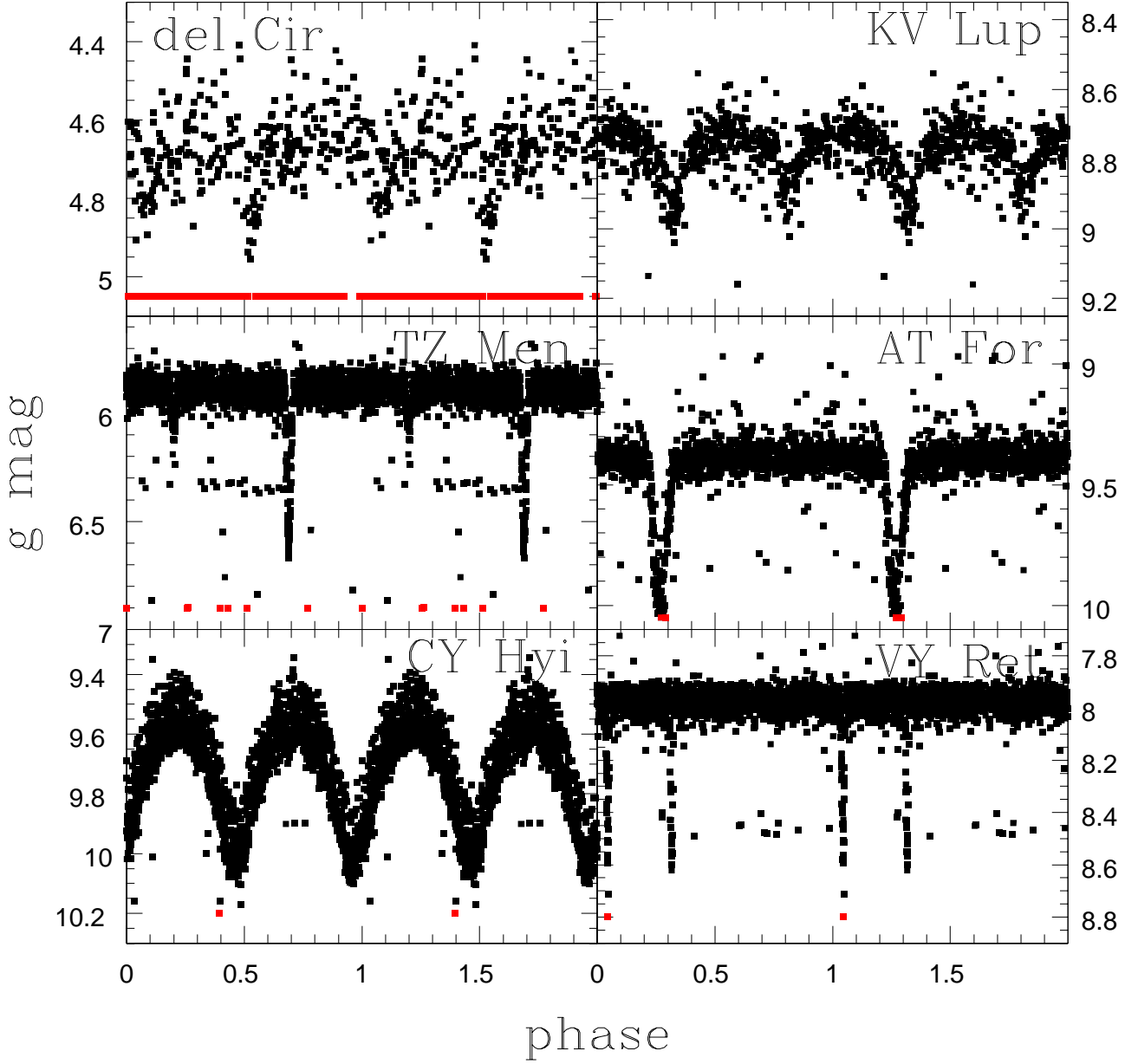


**Figure 11.** DNN light curves of the eclipsing binaries from Figs. 8 and 9 (black squares) as compared to their light curves using both V and g band data from all the ASAS-SN cameras observing each star. Outliers are marked at the bottom in red.

This is seen to a lesser extent for W Sgr where too few faint outliers were rejected for the good parts of the light curves to be perfectly lined up. But for R Cae, S Tuc and the eclipsing binaries in Fig. 11, the results are extremely good.

## 5. CONCLUSIONS AND FUTURE WORK

We developed a deep neural network (DNN) for the accurate photometry of saturated stars. The network was trained using predictions for the counts produced by the target star in a sample of  $\sim 332$  thousand postage stamp

images of stars roughly uniformly spread in magnitude from  $g \sim 3$  to 15 mag. For the verification sample there is little bias in the magnitude estimates except for the fainter stars, and 68% (95%) of the magnitude differences are less than 0.12 (0.34) mag (see Fig. 3). More importantly, the typical scatter in the light curve of a saturated star is only 0.037 mag (half the 15 to 85 percentile range about the mean) compared to 0.22 mag for the SP2 light curves (see Fig. 4). The DNN light curves of many bright variable stars are dramatically better

than their SP2 light curves (see Figs. 6 to 9) although the performance can some times be poor, as illustrated by the naked eye Cepheids in Fig. 7 (see below). Although the network was trained using data from only one camera, it appears to work equally well when tested using data from all cameras and both V and g band data when combined using a Gaussian process to intercalibrate the light curve means (see Figs. 10, 11). For some systems, this calibration procedure and/or outlier rejection would have to be done more carefully, but the results are otherwise very encouraging.

We analyzed the reduced ASAS-SN images interpolated to the frame of the reference image. Using the interpolated images meant that the pixel location of the target stars was fixed and could be accurately determined from the well-verified astrometry of the reference images (2 arcsec errors relative to Tycho stars at worst, compared to a 16 arcsec FWHM). We do not see any evidence that the interpolation causes problems.

Using the as-reduced images creates the problems seen for the bright Cepheids because of two issues. The first is that an interplay between adding bias corrections and the inheritance from the ASAS pipeline of reading only integer fits files can lead to damaging saturated images because of integer overflows. This manifests as pixels in the star being flagged as bad and given a pixel value of unity. This obviously causes severe problems for the standard aperture photometry pipeline. The DNN pipeline largely manages to correctly interpret the flagged pixels and recover a good estimate of the true flux. While we understand the origin of the problem, a fix is not trivial and has yet to be implemented. We believe the performance of a DNN retrained after the problem is fixed should be improved.

The second problem comes from mistakes made by the saturated star corrections inherited from the ASAS pipeline. As noted earlier, the pipeline tries to collect the flux from the bleed trail and add it as a Gaussian at the location of the saturated star with the FWHM of the data. This generally works very well, but the flux is sometimes assigned to the wrong location and sometimes seems not to be assigned to any location. We see this problem here for the very brightest examples we show (Figs. 7, 10, 11). Determining the origin of these problems in the pipeline is beyond our present scope.

We suspect that our approach would have worked well and avoided this problem using data without these attempts to correct saturated stars. Testing this is, however, an involved process. The original raw images are available, but they would have to be reprocessed without the saturated star corrections (or at least the postage stamp images needed for each star would have to be

reprocessed). The pixel positions of stars would also now vary from image to image, so we would need to be fully confident of the astrometry of the individual images. Checking this astrometry has not been a priority because all the current ASAS-SN results depend only on the astrometry of the reference image for a field and not on the astrometry of the individual images.

One likely area where our results could be improved is in the estimation of the predicted counts for the training set. As a reminder, we predicted SDSS g magnitudes from Gaia DR3 magnitudes, converted them to counts using the zero point of the ASAS-SN reference image and the image subtraction estimate of the transparency difference between the images defining the zero point and the current image, and attempted to correct for the flux from other stars within the large ASAS-SN PSF. The [Riello et al. \(2021\)](#) transformation from Gaia magnitudes to g band is not great, with a reported scatter of 0.075 mag. This is, however, not large enough to be a major contributor to the scatter seen for the verification data. Nonetheless, it might be better to have used ATLAS REFCAT ([Tonry et al. 2018b](#)) since it was built in part to systematically estimate g band magnitudes.

The crowding corrections were computed based only on the Gaia G band magnitudes, and they should probably have been based on the estimated g band magnitudes. The thought was that these corrections should mostly be small, so modest fractional errors in them would not be important. Retrospectively, this may be need to be treated more carefully for the non-saturated stars. For the saturated stars which are the primary target of the project, this is less of an issue simply because the stars are so bright and the standard pipeline performs so poorly. Moreover, the scatter seen for the unsaturated stars in the verification data does not seem to depend on Galactic latitude, which suggests that problems with confusion cannot be a dominant driver of the scatter.

If a primary driver of the scatter was simply the accuracy of the conversion from estimated counts to magnitudes driven by zero point and transparency errors, then we would expect the fluctuations in the light curves of constant sources lying in the same field to be correlated. If so, this would then lead to a natural approach to improving the image calibrations by using the correlated variability to estimate an image calibration correction. We inspected this question for the trial light curves of non-varying sources lying in the same field and found, unfortunately, no obvious correlations.

Probably the most important issues to be addressed are the problems created by the ASAS-SN pipeline, fixing the damage done to saturated stars and either under-

standing the failures of the saturated star corrections or switching to using images without the corrections. We need to more extensively test how well the DNN works on multiple cameras to determine if we can simply train a single DNN for all cameras, perhaps with the camera identification as an additional item of metadata.

This method is now available as an option on ASAS-SN Sky Patrol v1.0 (<https://asas-sn.osu.edu/>, Kochanek et al. 2017) as the “Saturated Stars (Machine Learning)” photometry option. As should be clear from the examples, the results become less predictable for stars approaching naked eye visibility and brighter. The present method supplies no magnitude uncertainties, so these are simply reported as the typical scatter seen in Fig. 4. Better error estimates of the relative errors can be derived from the light curves, but this requires some information on the nature of any variability (e.g. pe-

riodic or non-periodic), making it difficult to estimate automatically. We anticipate that the machine learning results will steadily improve, particularly once the reduction pipeline problems for saturated stars are corrected. It is also considerably faster than the most equivalent mode of Sky Patrol v1.0 (“Aperture Photometry”), which takes roughly 5 times longer to produce the light curves shown in Figs. 6-9.

We thank Dustin Perzanowski of Ohio State’s ASCTech group for adding the machine learning option to Sky Patrol v1.0. CSK is supported by NSF grants AST-2307385 and AST-1908570. ASAS-SN is funded in part by the Gordon and Betty Moore Foundation through grants GBMF5490 and GBMF10501 to the Ohio State University, and also funded in part by the Alfred P. Sloan Foundation grant G-2021-14192.

## REFERENCES

- Abdurro’uf, Accetta, K., Aerts, C., et al. 2022, *ApJS*, 259, 35, doi: [10.3847/1538-4365/ac4414](https://doi.org/10.3847/1538-4365/ac4414)
- Alard, C. 2000, *A&AS*, 144, 363, doi: [10.1051/aas:2000214](https://doi.org/10.1051/aas:2000214)
- Alard, C., & Lupton, R. H. 1998, *ApJ*, 503, 325, doi: [10.1086/305984](https://doi.org/10.1086/305984)
- Bellm, E. C., Kulkarni, S. R., Graham, M. J., et al. 2019, *PASP*, 131, 018002, doi: [10.1088/1538-3873/aaecbe](https://doi.org/10.1088/1538-3873/aaecbe)
- Eyer, L., Audard, M., Holl, B., et al. 2023, *A&A*, 674, A13, doi: [10.1051/0004-6361/202244242](https://doi.org/10.1051/0004-6361/202244242)
- Gaia Collaboration, Prusti, T., de Bruijne, J. H. J., et al. 2016, *A&A*, 595, A1, doi: [10.1051/0004-6361/201629272](https://doi.org/10.1051/0004-6361/201629272)
- Gaia Collaboration, Vallenari, A., Brown, A. G. A., et al. 2023, *A&A*, 674, A1, doi: [10.1051/0004-6361/202243940](https://doi.org/10.1051/0004-6361/202243940)
- Hart, K., Shappee, B. J., Hey, D., et al. 2023, *arXiv e-prints*, arXiv:2304.03791, doi: [10.48550/arXiv.2304.03791](https://doi.org/10.48550/arXiv.2304.03791)
- Ivezić, Ž., Kahn, S. M., Tyson, J. A., et al. 2019, *ApJ*, 873, 111, doi: [10.3847/1538-4357/ab042c](https://doi.org/10.3847/1538-4357/ab042c)
- Jayasinghe, T., Stanek, K. Z., Kochanek, C. S., et al. 2019, *MNRAS*, 486, 1907, doi: [10.1093/mnras/stz844](https://doi.org/10.1093/mnras/stz844)
- Kim, E. J., & Brunner, R. J. 2017, *Monthly Notices of the Royal Astronomical Society*, 464, 4463, doi: [10.1093/mnras/stw2672](https://doi.org/10.1093/mnras/stw2672)
- Kingma, D. P., & Ba, J. 2017, *Adam: A Method for Stochastic Optimization*, *arXiv*, <http://arxiv.org/abs/1412.6980>
- Kochanek, C. S., Shappee, B. J., Stanek, K. Z., et al. 2017, *PASP*, 129, 104502, doi: [10.1088/1538-3873/aa80d9](https://doi.org/10.1088/1538-3873/aa80d9)
- Kozłowski, S., Kochanek, C. S., Udalski, A., et al. 2010, *ApJ*, 708, 927, doi: [10.1088/0004-637X/708/2/927](https://doi.org/10.1088/0004-637X/708/2/927)
- Page, M. J., Kuin, N. P. M., Breeveld, A. A., et al. 2013, *MNRAS*, 436, 1684, doi: [10.1093/mnras/stt1689](https://doi.org/10.1093/mnras/stt1689)
- Pasquet, J., Bertin, E., Treyer, M., Arnouts, S., & Fouchez, D. 2019, *Astronomy & Astrophysics*, 621, A26, doi: [10.1051/0004-6361/201833617](https://doi.org/10.1051/0004-6361/201833617)
- Paszke, A., Gross, S., Massa, F., et al. 2019, in *Advances in Neural Information Processing Systems* 32, ed. H. Wallach, H. Larochelle, A. Beygelzimer, F. d’Alché Buc, E. Fox, & R. Garnett (Curran Associates, Inc.), 8024–8035. <http://papers.neurips.cc/paper/9015-pytorch-an-imperative-style-high-performance-differentiable-library>
- Pojmanski, G. 2002, *AcA*, 52, 397, doi: [10.48550/arXiv.astro-ph/0210283](https://doi.org/10.48550/arXiv.astro-ph/0210283)
- Qu, H., Sako, M., Möller, A., & Dux, C. 2022, *Machine Learning for Astrophysics*, 51
- Riello, M., De Angeli, F., Evans, D. W., et al. 2021, *A&A*, 649, A3, doi: [10.1051/0004-6361/202039587](https://doi.org/10.1051/0004-6361/202039587)
- Shappee, B. J., Prieto, J. L., Grupe, D., et al. 2014, *ApJ*, 788, 48, doi: [10.1088/0004-637X/788/1/48](https://doi.org/10.1088/0004-637X/788/1/48)
- Su, K. Y. L., Rieke, G. H., Marengo, M., & Schlawin, E. 2022, *AJ*, 163, 46, doi: [10.3847/1538-3881/ac3b5e](https://doi.org/10.3847/1538-3881/ac3b5e)
- Tonry, J. L., Denneau, L., Heinze, A. N., et al. 2018a, *PASP*, 130, 064505, doi: [10.1088/1538-3873/aabadf](https://doi.org/10.1088/1538-3873/aabadf)
- Tonry, J. L., Denneau, L., Flewelling, H., et al. 2018b, *ApJ*, 867, 105, doi: [10.3847/1538-4357/aae386](https://doi.org/10.3847/1538-4357/aae386)
- Yang, Z., Liu, M., Yuan, H., et al. 2023, *The Astronomical Journal*, 166, 210, doi: [10.3847/1538-3881/acfeed](https://doi.org/10.3847/1538-3881/acfeed)
- Yuan, H., Liu, M., Yang, Z., et al. 2023, *The Astronomical Journal*, 166, 244, doi: [10.3847/1538-3881/ad0297](https://doi.org/10.3847/1538-3881/ad0297)

Zhou, H., Jin, Z.-P., Covino, S., Fan, Y.-Z., & Wei, D.-M.  
2023, arXiv e-prints, arXiv:2308.10171,  
doi: [10.48550/arXiv.2308.10171](https://doi.org/10.48550/arXiv.2308.10171)